



Controlling Lattice Misfit and Creep Rate Through the γ' Cube Shapes in the $\text{Al}_{10}\text{Co}_{25}\text{Cr}_8\text{Fe}_{15}\text{Ni}_{36}\text{Ti}_6$ Compositionally Complex Alloy with Hf and W Additions

Y. Yesilcicek¹ · S. Haas² · P. Suárez Ocaño¹ · E. Zaiser^{3,4} · R. Hesse¹ · D. M. Többens⁴ · U. Glatzel² · A. M. Manzoni^{1,4}

Received: 24 June 2022 / Accepted: 2 November 2022
© The Author(s) 2022

Abstract

Trace elements play an important role in the fine-tuning of complex material properties. This study focuses on the correlation of microstructure, lattice misfit and creep properties. The compositionally complex alloy $\text{Al}_{10}\text{Co}_{25}\text{Cr}_8\text{Fe}_{15}\text{Ni}_{36}\text{Ti}_6$ (in at. %) was tuned with high melting trace elements Hf and W. The microstructure consists of a γ matrix, γ' precipitates and the Heusler phase and it is accompanied by good mechanical properties for high temperature applications. The addition of 0.5 at.% Hf to the $\text{Al}_{10}\text{Co}_{25}\text{Cr}_8\text{Fe}_{15}\text{Ni}_{36}\text{Ti}_6$ alloy resulted in more sharp-edged cubic γ' precipitates and an increase in the Heusler phase amount. The addition of 1 at.% W led to more rounded γ' precipitates and the dissolution of the Heusler phase. The shapes of the γ' precipitates of the alloys $\text{Al}_{9.25}\text{Co}_{25}\text{Cr}_8\text{Fe}_{15}\text{Ni}_{36}\text{Ti}_6\text{Hf}_{0.25}\text{W}_{0.5}$ and $\text{Al}_{9.25}\text{Co}_{25}\text{Cr}_8\text{Fe}_{15}\text{Ni}_{36}\text{Ti}_6\text{Hf}_{0.5}\text{W}_{0.25}$, that are the alloys of interest in this paper, create a transition from the well-rounded precipitates in the alloy with 1% W containing alloy to the sharp angular particles in the alloy with 0.5% Hf. While the lattice misfit has a direct correlation to the γ' precipitates shape, the creep rate is also related to the amount of the Heusler phase. The lattice misfit increases with decreasing corner radius of the γ' precipitates. So does the creep rate, but it also increases with the amount of Heusler phase. The microstructures were investigated by SEM and TEM, the lattice misfit was calculated from the lattice parameters obtained by synchrotron radiation measurements.

Keywords Lattice misfit · γ' precipitates shape · Creep properties · Compositionally complex alloys · High entropy alloys · Diffraction

Introduction

Since 1930 Ni-based superalloys have been the dominating materials class for applications at temperatures over 700 °C because of their stable microstructure, high strength, corrosion resistance and creep resistance over a great temperature

range. However, as the Ni production is environmentally challenging [1], the search for materials with a lower Ni-content yet equal or better properties remains one of the great challenges of the time. During the last 20 years, a new class of material called “high entropy alloys (HEA)” and “compositionally complex alloys (CCA)” have entered the materials world. While HEA consist of a single phase, CCAs have more than one phase. The idea behind this young class of materials is the design of materials with any desired properties since HEA consist of five or more principal elements with potentially unique features like high strength/hardness, outstanding wear resistance, exceptional high-temperature strength, good structural stability, good corrosion, and oxidation resistance [2]. In contrast to the HEA and CCA, the Ni-based superalloys have one main element, i.e., Ni, that is tuned with minor and trace elements. Apart from the main elements, HEA and CCA can also have concentrations of trace elements with less than 1 at.% to improve their properties and characteristics even further [3].

✉ Y. Yesilcicek
yasemin.yesilcicek@bam.de

¹ Bundesanstalt für Materialforschung und -Prüfung, Unter den Eichen 87, 12205 Berlin, Germany

² Metals and Alloys, University Bayreuth, Prof.-Rüdiger-Bormann-Str. 1, 95447 Bayreuth, Germany

³ Department of Materials Science and Technology, Technical University Berlin, Straße Des 17. Juni 135, 10623 Berlin, Germany

⁴ Institute of Applied Materials, Helmholtz-Zentrum Berlin, Hahn-Meitner-Platz 1, 14109 Berlin, Germany

This new class of alloys inspired scientists to create high-performance materials that can compete with Ni-base alloys at specific applications. In the authors' group the aimed for application parameters were temperatures around 700 °C and good creep resistance as can be found in the medium temperature region of airplane turbines. Commercial Ni-based alloys that are used in this setting, e.g., Alloy 800H [4] and IN617 [5] will serve as a comparison in this study. During the first years of HEA and CCA research, the equiatomic AlCoCrCuFeNi CCA was very popular and much investigated. This CCA exhibits at least five phases and shows an overall very brittle behavior. In previous works calculations using Calphad based tools like Thermo-Calc [6] and databases like TTNi7 [7] combined with casting of promising alloys lead to an optimized concentration, i.e. Al₁₀Co₂₅Cr₈Fe₁₅Ni₃₆Ti₆ (at.%), from hereon called "the base alloy". The base alloy was chosen among 190 variations from the Al–Co–Cr–Cu–Fe–Ni–Ti family because of its most promising mechanical properties [8]. The design idea behind the base alloy was explained in detail in Ref. [8] and is not included in the scope of this paper. The base alloy consist of three phases: the γ matrix of A1 type structure, γ' precipitates of L1₂ types structure and a Heusler phase of L2₁ type structure, which was intensely studied in previous works [8, 9]. The obtained mechanical properties are superior to those of other well-studied HEAs and CCAs like equiatomic CoCrFeMnNi [10] or AlCoCrCuFeNi [11] and of several commercial Ni-based superalloys like Alloy 800H and IN617 [12–14]. Studies have shown that the addition of single trace elements can tune the alloy's properties towards one or the other direction [13, 15]. Besides the microstructure, the mechanical properties at elevated temperatures are improved by additions of high melting elements, even in small amounts [16]. Trace elements of Y, W, Zr, Hf and Mo have been added to the base alloy and the improvements in microstructure and thus the mechanical properties have been recorded in previous works [15–17], but until now no studies are known about the combination of two such trace elements with different influence. While adding Hf to the base alloy results in more cuboidal γ' precipitates and more roundish Heusler phases, the addition of W induces a more rounded, spherical γ' precipitates shape [13, 17] and the dissolution of the Heusler phase.

This publication investigates the influence of trace element additions of 0.25–0.5 at.% Hf and W on the compositionally complex alloy Al₁₀Co₂₅Cr₈Fe₁₅Ni₃₆Ti₆, both from a microstructural and a mechanical perspective and the correlation of both. Creep tests are chosen as a means of simulating the long-term stress on the material in use. Two alloys with the following compositions have been newly cast: Al_{9.25}Co₂₅Cr₈Fe₁₅Ni₃₆Ti₆Hf_{0.25}W_{0.5} and Al_{9.25}Co₂₅Cr₈Fe₁₅Ni₃₆Ti₆Hf_{0.5}W_{0.25}. The main focus of the microstructural investigation lies on the shape of the γ'

precipitates and the lattice misfit of γ - γ' . They are investigated via electron microscopy and synchrotron X-ray diffraction.

Experimental/Materials and Methods

Sample Preparation

The alloys were cast in two different ways, i.e., as polycrystalline ingots for microstructural analysis whereas the creep samples were directionally solidified. All concentration values are given in at.%. To obtain the polycrystalline CCAs Al_{9.25}Co₂₅Cr₈Fe₁₅Ni₃₆Ti₆Hf_{0.25}W_{0.5} and Al_{9.25}Co₂₅Cr₈Fe₁₅Ni₃₆Ti₆Hf_{0.5}W_{0.25}, elements of at least 99.99% purity have been weighed and melted in an induction levitation furnace under argon atmosphere to form ingots of about 20 g. To ensure homogeneous distribution of the elements, the alloys were remelted several times and cooled inside the furnace. Ingots for creep tests were prepared from 99.99% pure elements Al, Co, Cr, Fe and Ti, and of pre-alloyed buttons consisting of the trace elements and Ni. The latter were prepared by arc-melting. The directional solidification was achieved via the Bridgman process. The pure elements and the pre-alloyed buttons were melted by induction and cast into a hot mould, keeping the alloy liquid. The [100] orientation of the grains was obtained by a slow, 3 mm/s solidification rate, where the melt is pulled through a water-cooled baffle. The ingots formed are 110 mm long and have a diameter of 20 mm. For more details, see [16].

The chosen heat treatment parameters are listed in Table 1 and complemented by the ones already known for the base alloy, Al₉Co₂₅Cr₈Fe₁₅Ni₃₆Ti₆W₁ and Al_{9.5}Co₂₅Cr₈Fe₁₅Ni₃₆Ti₆Hf_{0.5} [14, 16]. Abbreviations are used to simplify reading. Each heat treatment was carried out in pure argon atmosphere and the samples were cooled inside the furnace afterwards. The different homogenization temperatures are due to the formation of a eutectic phase in the alloys containing Hf, which should be avoided (see Ref. [18]).

Samples of approximately 2 mm thickness were embedded, ground and polished using a diamond suspension with 1 μ m particle sizes. The final polishing was performed using an oxide polishing suspension (OPS) with 200 nm particle size. Samples for scanning electron microscopy (SEM) were etched with an etching solution of 3 g Mo-acid in 100 ml H₂O, 100 ml HCl and 100 ml HNO₃. Samples for transmission electron microscopy (TEM) were mounted on a parallel specimen holder and ground on both sides to a thickness of 100 μ m using a grit size of P1200. Samples were punched to obtain 3 mm diameter discs. Electropolishing was carried out in a Struers TenuPol 3 with a solution of 83 vol.

Table 1 Parameters for the heat treatment of the five alloys, $\text{Al}_{10}\text{Co}_{25}\text{Cr}_8\text{Fe}_{15}\text{Ni}_{36}\text{Ti}_6$, $\text{Al}_{9.5}\text{Co}_{25}\text{Cr}_8\text{Fe}_{15}\text{Ni}_{36}\text{Ti}_6\text{Hf}_{0.5}$, $\text{Al}_{9.25}\text{Co}_{25}\text{Cr}_8\text{Fe}_{15}\text{Ni}_{36}\text{Ti}_6\text{Hf}_{0.25}\text{W}_{0.5}$, $\text{Al}_{9.25}\text{Co}_{25}\text{Cr}_8\text{Fe}_{15}\text{Ni}_{36}\text{Ti}_6\text{Hf}_{0.5}\text{W}_{0.25}$ and $\text{Al}_9\text{Co}_{25}\text{Cr}_8\text{Fe}_{15}\text{Ni}_{36}\text{Ti}_6\text{W}_1$ CCAs

Alloy	Abbreviation	Homogenization	Annealing
$\text{Al}_{10}\text{Co}_{25}\text{Cr}_8\text{Fe}_{15}\text{Ni}_{36}\text{Ti}_6$	Base alloy	1220 °C/20 h	900 °C 50 h
$\text{Al}_{9.5}\text{Co}_{25}\text{Cr}_8\text{Fe}_{15}\text{Ni}_{36}\text{Ti}_6\text{Hf}_{0.5}$ [15]	Hf alloy	1130 °C/20 h	
$\text{Al}_{9.25}\text{Co}_{25}\text{Cr}_8\text{Fe}_{15}\text{Ni}_{36}\text{Ti}_6\text{Hf}_{0.5}\text{W}_{0.25}$	Hf _{0.5} W _{0.25} alloy	1130 °C/20 h	
$\text{Al}_{9.25}\text{Co}_{25}\text{Cr}_8\text{Fe}_{15}\text{Ni}_{36}\text{Ti}_6\text{Hf}_{0.25}\text{W}_{0.5}$	Hf _{0.25} W _{0.5} alloy	1130 °C/20 h	
$\text{Al}_9\text{Co}_{25}\text{Cr}_8\text{Fe}_{15}\text{Ni}_{36}\text{Ti}_6\text{W}_1$ [16]	W alloy	1220 °C/20 h	

% ethanol, 7 vol. % glycerin and 10 vol. % perchloric acid at -7 °C and 30 V.

Microstructural Characterization

Two types of optical microscopes (OM) were used to investigate the microstructure. The first is a reflected light microscope Reichert MeF3A, equipped with a Leica DFC 450 camera and operated with Lecia LES core version 4 software. The second OM is an Olympus GX71, an inverted microscope equipped with an Olympus SC50 microscope camera and operated with an Olympus image analysis software. Further detailed investigations with higher magnifications were done by using two SEMs. The first is a Tescan Vega 3 XLH operated at 20 keV. The second SEM is a Zeiss Sigma VP 300, operated at 15 keV and equipped with a Hikari Plus Electron backscatter diffraction (EBSD) camera.

TEM was performed in two instruments: The first is a JEOL JEM-2200FS Field Emission TEM operated at 200 kV. The second TEM is a Philips CM30 (ThermoFischer Scientific) operated at 300 kV. Bright field (BF), dark field (DF) and selected area diffraction (SAD) modes were used to show the γ' precipitates along their [100] direction, best suited to show their cubic shape.

Before synchrotron measurements, samples were oriented in a custom-built Laue diffractometer equipped with a tungsten X-ray tube operated at 25 kV. Large grains from the polycrystalline samples were marked with a permanent marker and their orientation transferred to the diffraction experiments.

Synchrotron diffraction was carried out at the KMC-2 beamline [19] at BESSY II in Berlin, Germany, using monochromatic radiation with an energy of 8048 eV, which corresponds to the Cu $K\alpha_1$ wavelength of 0.15406 nm. The proprietary high-vacuum furnace available at the beamline allowed to maintain 10^{-6} mbar up to a temperature of 930 °C, thus preventing oxidization of the sample surface. The selected beam size was $0.01 \times 0.01 \text{ mm}^2$. The use of a 2D detector allowed the measurement of the reciprocal space containing the selected Bragg peak [9]. Reflexes of the 200 and 300 lattice planes were measured to determine

the lattice parameters of the γ and γ' phases. The 300 reflexes were used to determine the γ' phase because the disordered γ phase has no 300 reflex, which made a distinction of the two phases possible (see e.g. Refs. [12, 20] for more details). Lattice parameters for γ and γ' were calculated for all temperatures (room temperature, 200, 500, 830, 880 and 930 °C). For peak fitting of the 200 and 300 reflexes, the Origin® software was used [21].

Volume fractions of Heusler phase and γ' phase as well as precipitates size of γ' phase were quantified by means of OM and SEM image analysis with the software Fiji [22]. Phase segmentation was carried out via trainable weka segmentation [23].

Creep Measurements

Creep measurements were performed on flat, directionally solidified samples that were prepared via electro discharge wire cutting. The z-axis of the sample corresponds to the [100] growth direction and the dimensions are as follows: $1.0 \times 1.9 \text{ mm}^2$ cross-section, 8 mm gauge length and 25 mm total length. Small markers allow for a high-resolution camera detection of the elongation. The erosion layer was removed via grinding and final cleaning took place in the ultrasonic bath.

The furnace used for creep experiments was self-built and has been described in detail in Ref [24]. The temperature chosen for creep experiments was 750 °C and the load was adapted to the cross section, resulting in stresses of 375 and 425 MPa. Experiments in this work were combined with former experiments in which additional stresses were investigated (see [16]).

Results and Discussion

The microstructures of the base, the Hf and the W alloys in polycrystalline state have been published previously before [9, 12, 13, 16]. The base and the Hf alloys are characterized by a large volume fraction of a γ - γ' microstructure and several volume % of Heusler phase, needle-shaped in case of the base alloy and irregularly shaped in case of the Hf

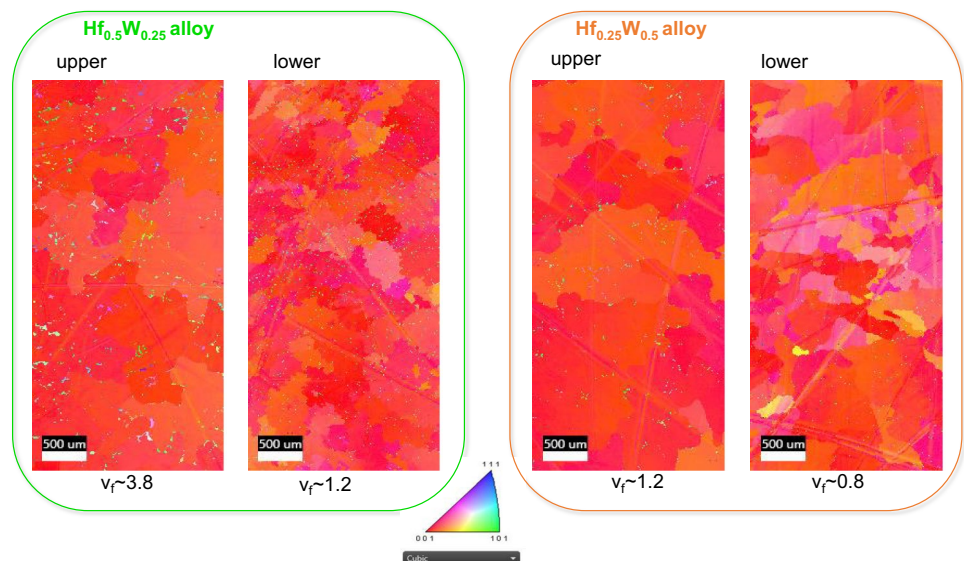
alloy. The W alloy shows hardly any Heusler phase but a few at the grain boundaries. The mixed alloys follow the overall microstructure of the Hf alloy. The volume fractions of the γ , γ' and the Heusler phase of the $\text{Hf}_{0.25}\text{W}_{0.5}$ alloy and the $\text{Hf}_{0.5}\text{W}_{0.25}$ alloy are listed in Table 2.

An observation of the grain structure of the directionally solidified samples by EBSD (shown in Fig. 1, see Supplementary Information Figure S1 for image quality maps) revealed their large sizes up to several mm and the successful orientation in the [100] direction by the Bridgman process, made visible by the overall reddish color palette. The Heusler phase is displayed in green and light purple, i.e. along the $[101]_{L21}$ and $[112]_{L21}$ directions. It was found that the upper (last solidified) and the lower (first solidified) ends of the ingots showed a slightly different grain and phase morphology, i.e. grain sizes were larger at the upper ends of the ingot, as was the volume fraction of the Heusler phase. The latter is particularly important in case of the $\text{Hf}_{0.5}\text{W}_{0.25}$ alloy: the upper end shows a Heusler volume fraction of about 3.8 vol.% and the lower end about 1.2 vol.%. For comparison: the Heusler volume fraction in the base alloy is around 3 vol.% [9], that in the Hf alloy around 6 vol.% [13] and that in the W alloy negligible (< 1 vol.%).

Table 2 Volume fractions of the γ , γ' and Heusler phase for the $\text{Hf}_{0.25}\text{W}_{0.5}$ alloy and the $\text{Hf}_{0.5}\text{W}_{0.25}$ alloy

Volume fractions [%]	γ -phase	γ' -phase	Heusler phase
$\text{Hf}_{0.25}\text{W}_{0.5}$ alloy	44.6 ± 1.5	50.6 ± 1.3	4.8 ± 1.6
$\text{Hf}_{0.5}\text{W}_{0.25}$ alloy	43.1 ± 1.8	51.9 ± 2.0	5.0 ± 1.5

Fig. 1 EBSD observation of the upper and the lower ingot ends of the two mixed alloys, $\text{Hf}_{0.5}\text{W}_{0.25}$ and $\text{Hf}_{0.25}\text{W}_{0.5}$ and the volume fractions v_f of the Heusler phase



Microstructure and Lattice Parameters

Figure 2 shows SEM images of the microstructure of the $\text{Hf}_{0.25}\text{W}_{0.5}$ alloy and $\text{Hf}_{0.5}\text{W}_{0.25}$ alloys. Both alloys show the irregularly shaped Heusler phase inside a matrix consisting of γ and γ' , as can also be seen in the Hf alloy [16]. The W alloy hardly shows any Heusler phase, except at the grain boundaries (compare Ref. [16]).

In Fig. 3 DF TEM images show the microstructures of the four alloy variations. They show a continuous change in γ' shape from high to low Hf content, or low to high W content, respectively. The TEM images were recorded along the [001] zone axis, where the cubic shape can be distinguished best. The γ' precipitates in the Hf alloy (a) have the most angular edges, followed by the $\text{Hf}_{0.5}\text{W}_{0.25}$ alloy (b). The shape of the γ' phase in the $\text{Hf}_{0.25}\text{W}_{0.5}$ alloy (c), where W is more present than Hf, is rounded but not as much as in the alloy with 1 at. % W (d). The shapes of the γ' precipitates of the alloys $\text{Hf}_{0.25}\text{W}_{0.5}$ and $\text{Hf}_{0.5}\text{W}_{0.25}$ make a transition from the well-rounded precipitates in the W alloy to the sharp angular precipitates in the Hf alloy. Figure 3 is a confirmation of previously determined partitioning of the trace element Hf to the γ' precipitates [17], while W is rather neutral with only a slight preference of partitioning into the γ matrix.

Figure 4 shows the increase in lattice parameter of both phases (a) γ and (b) γ' for the five alloys as a function of temperature. The crystal lattice tends to expand linearly with temperature due to thermal expansion. In both phases and for almost all alloys the lattice parameters are higher than in the base alloy (black line). Concluding from this, it can be said that even though Hf and W have their preferred diffusion phases (γ' for Hf, γ for W), they diffuse into other

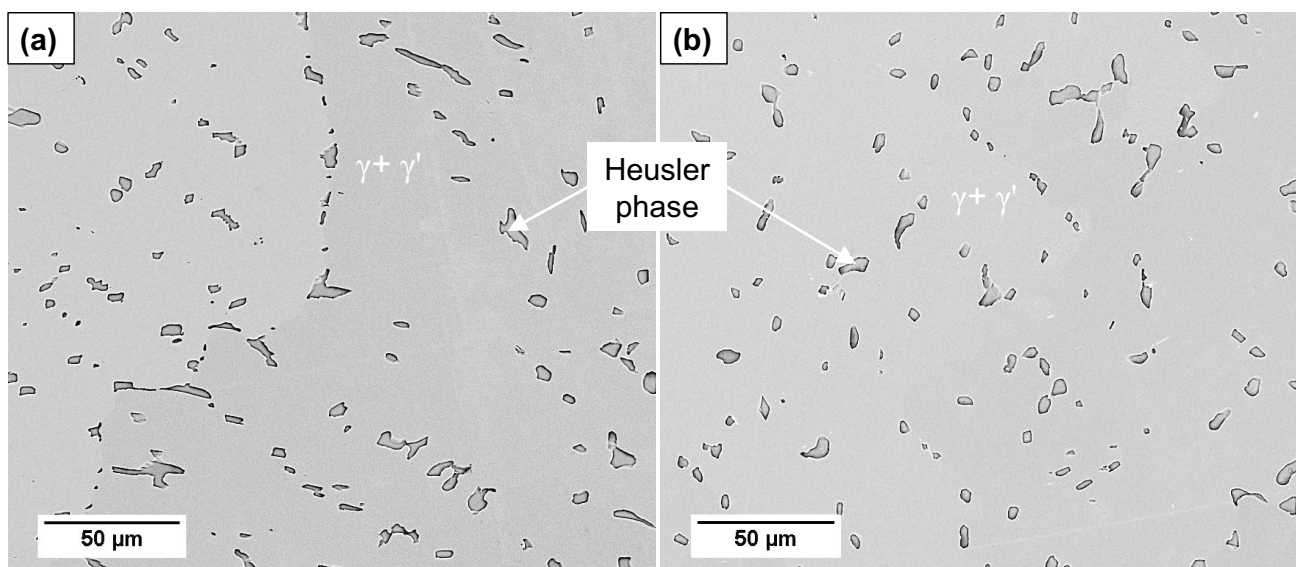


Fig. 2 SEM secondary electron images of **a** $\text{Hf}_{0.25}\text{W}_{0.5}$ and **b** the $\text{Hf}_{0.5}\text{W}_{0.25}$ alloys after homogenisation and subsequent aging showing the Heusler phases inside a matrix of γ and γ'

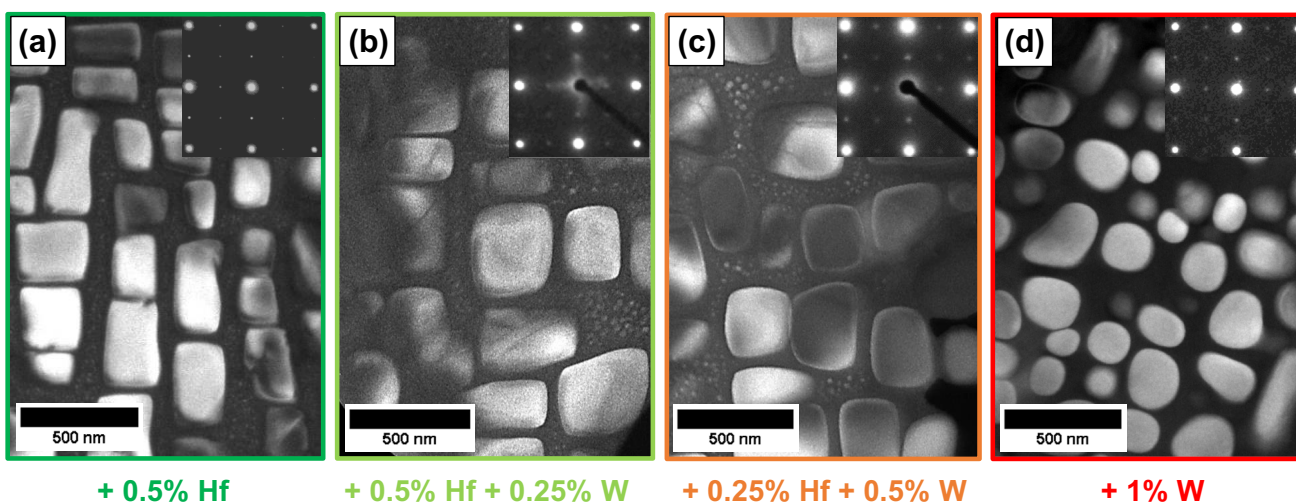


Fig. 3 TEM DF images showing the γ' morphology of **a** Hf alloy, **b** $\text{Hf}_{0.5}\text{W}_{0.25}$ alloy, **c** $\text{Hf}_{0.25}\text{W}_{0.5}$ alloy and **d** W alloy after homogenization and subsequent aging. The images are obtained using the (110)

super lattice diffraction spot and the respective SAD patterns taken along the [100] zone axis which are positioned in the top right corner

phase, too, and expand its lattice parameter through their larger atomic size.

To determine the coherency between γ and γ' , the lattice misfit (δ) will be calculated by Eq. 1, where $a_{\gamma'}$ and a_{γ} are the lattice parameters of the γ' and γ phase, respectively.

$$\delta = 2 \frac{a_{\gamma'} - a_{\gamma}}{a_{\gamma'} + a_{\gamma}} \quad (1)$$

Figure 5 shows the evolution of all lattice misfits as a function of temperature for the following alloys: base alloy, W alloy, $\text{Hf}_{0.25}\text{W}_{0.5}$ alloy, $\text{Hf}_{0.5}\text{W}_{0.25}$ alloy and the Hf alloy. The magnitude of $|\delta|$ is highest at low temperatures and lower at high temperatures for all alloys. This means that the difference between the lattice parameters between the phases γ - γ' decreases while temperature increases. According to Svoboda et al. [25] this circumstance is desired in terms of obtaining better creep properties. The misfit data for the base alloy is shown in black and can be

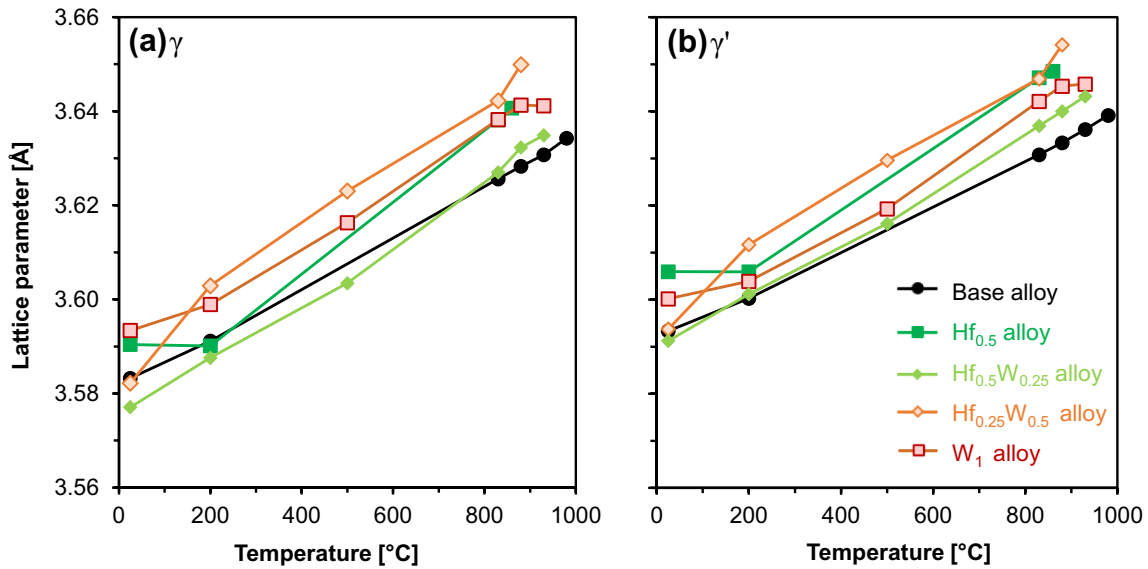


Fig. 4 Evolution of γ and γ' phases as a function of temperature of the base alloy $\text{Al}_{10}\text{Co}_{25}\text{Cr}_8\text{Fe}_{15}\text{Ni}_{36}\text{Ti}_6$ (black) and the modified alloys $\text{Al}_{9.5}\text{Co}_{25}\text{Cr}_8\text{Fe}_{15}\text{Ni}_{36}\text{Ti}_6\text{Hf}_{0.5}$ (dark green), $\text{Al}_{9.25}\text{Co}_{25}\text{Cr}_8\text{Fe}_{15}\text{Ni}_{36}\text{Ti}_6\text{Hf}_{0.25}\text{W}_{0.25}$ (bright green), $\text{Al}_{9.25}\text{Co}_{25}\text{Cr}_8\text{Fe}_{15}\text{Ni}_{36}\text{Ti}_6\text{Hf}_{0.25}\text{W}_{0.5}$ (orange) and $\text{Al}_{9.25}\text{Co}_{25}\text{Cr}_8\text{Fe}_{15}\text{Ni}_{36}\text{Ti}_6\text{W}_1$ (red). Partially adapted from [17]

$\text{Al}_{9.25}\text{Co}_{25}\text{Cr}_8\text{Fe}_{15}\text{Ni}_{36}\text{Ti}_6\text{Hf}_{0.25}\text{W}_{0.5}$ (orange) and $\text{Al}_{9.25}\text{Co}_{25}\text{Cr}_8\text{Fe}_{15}\text{Ni}_{36}\text{Ti}_6\text{W}_1$ (red). Partially adapted from [17]

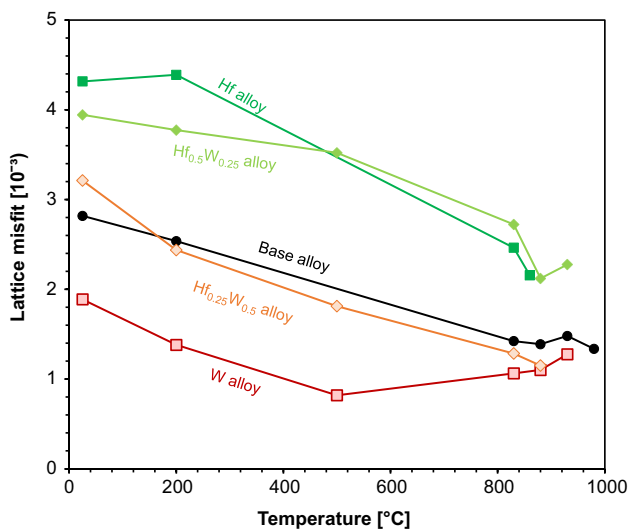


Fig. 5 The evolution of lattice misfit over temperature of the base alloy $\text{Al}_{10}\text{Co}_{25}\text{Cr}_8\text{Fe}_{15}\text{Ni}_{36}\text{Ti}_6$ (black) and the modified alloys $\text{Al}_{9.5}\text{Co}_{25}\text{Cr}_8\text{Fe}_{15}\text{Ni}_{36}\text{Ti}_6\text{Hf}_{0.5}$ (dark green), $\text{Al}_{9.25}\text{Co}_{25}\text{Cr}_8\text{Fe}_{15}\text{Ni}_{36}\text{Ti}_6\text{Hf}_{0.25}\text{W}_{0.25}$ (bright green), $\text{Al}_{9.25}\text{Co}_{25}\text{Cr}_8\text{Fe}_{15}\text{Ni}_{36}\text{Ti}_6\text{Hf}_{0.25}\text{W}_{0.5}$ (orange) and $\text{Al}_{9.25}\text{Co}_{25}\text{Cr}_8\text{Fe}_{15}\text{Ni}_{36}\text{Ti}_6\text{W}_1$ (red). Partially adapted from [17]

considered as the reference curve. The γ' phase preferring trace element containing alloys, i.e. the Hf alloy, has a higher misfit compared to the base alloy. The alloy which contains the γ matrix preferring trace element, i.e. the W alloy, has a lower lattice misfit than the base alloy. The

$\text{Hf}_{0.25}\text{W}_{0.5}$ and $\text{Hf}_{0.5}\text{W}_{0.25}$ alloys show lattice misfits that lie between the lattice misfits of the Hf and W alloys.

The shape of the γ' phase has a direct link to the lattice misfit of $\gamma - \gamma'$. It is known from previous studies that a mismatch magnitude of $0 < |\delta| < 0.2 \times 10^{-3}$ encourages spherical precipitates, a mismatch magnitude $0.5 \times 10^{-3} < |\delta| < 1.0 \times 10^{-3}$ generates cuboidal precipitates and mismatch magnitude $|\delta| > 1.25 \times 10^{-3}$ results in plate-like precipitates [26]. As trace elements like Hf are added and the lattice mismatch increases, the change to cuboidal shape is encouraged due to the necessity to minimize the elastic energy [26, 27]. In our study, the largest misfits go along with the edgiest γ' precipitates and vice versa, as has been reported for Ni- and Co-based superalloys [28]. However, Ni-based superalloys possess mostly negative misfits at room temperature and become more negative as the temperature increases, resulting in an increase in lattice misfit magnitude with temperature. Co-based superalloys usually exhibit a positive lattice misfit which decreases in magnitude as the temperature increases [28], like the CCAs presented in this manuscript.

Mughrabi et al. [28] proposed that alloys with a positive misfit could possibly provide better high-temperature strength, especially better creep properties, compared to similar alloys with a negative misfit. The lattice misfit shows the difference in lattice parameter of the phases γ and γ' . At high temperatures this value decreases and gets closer to 0, in the case, if the lattice misfit is positive. In this case the coherency stresses will be minimized leading to decrease the driving force for microstructural destabilization [28].

This work has shown that all modified alloys have a positive misfit at all temperatures and the magnitude of the lattice misfit decreases with temperature. The positive lattice misfit makes these alloys the candidates for high-temperature applications in the future.

Creep Properties

Figure 6 shows the creep curves of the a) $Hf_{0.5}W_{0.25}$ (green) and b) the $Hf_{0.25}W_{0.5}$ (orange) alloys determined for two stresses, i.e. 375 (dark colour) and 425 MPa (bright colour). Unlike those determined for the Hf and the W alloys (not shown here, see [16]), these curves look different for samples cut from the upper (straight line) and the lower (dashed line) part of the ingot. This is in agreement with the microstructural observations made in Fig. 1: the upper end of the ingots show different grain sizes and an increased amount of Heusler phases, especially in case of the $Hf_{0.5}W_{0.25}$ alloy

(Fig. 1a). The creep experiments carried out with samples from the upper end of the ingot show an inferior creep resistance.

The minimum creep rate from the secondary creep stage is determined for both mixed alloys and compared to those of the base, the Hf and the W alloys (published earlier [16]). Figure 7 shows the Norton plot of the five alloys.

The base alloy shows the highest creep rates at a given stress. Addition of any trace element enhances the creep response by about 13% for the lowest creep rates. The two alloys with both Hf and W show very similar creep behaviour, situated between the alloys with only Hf or W. The trend in creep response follows the trend of the γ' particle shape: the more cubic the γ' precipitate, the better the creep resistance.

The most prominent feature in the graph, i.e. the different Norton exponent in case of the W alloy, has been explained before [16]. The almost complete absence of the Heusler

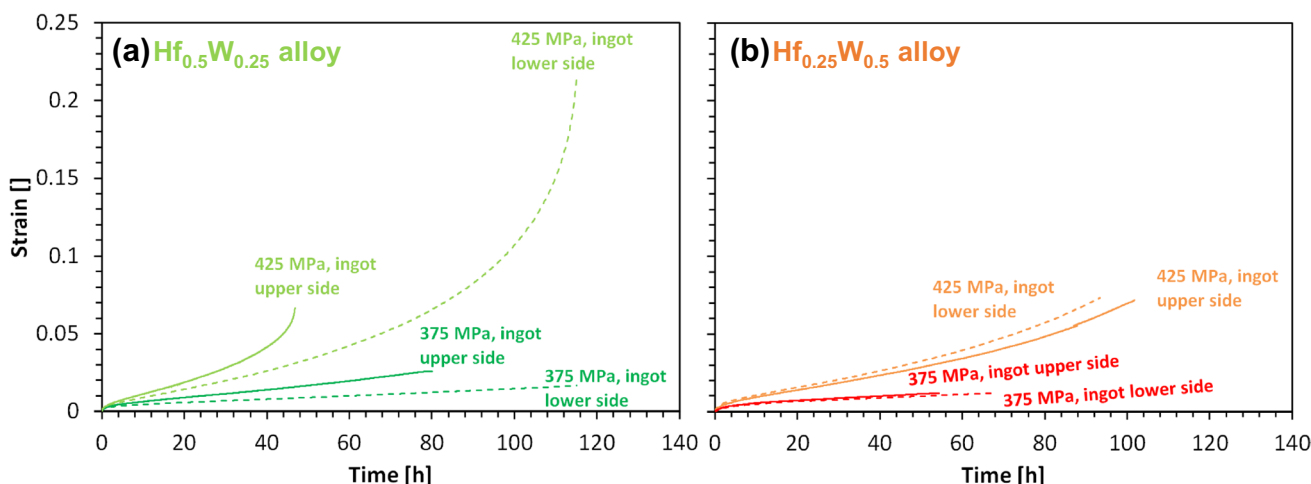


Fig. 6 Creep curves from a) the $Hf_{0.5}W_{0.25}$ and b) the $Hf_{0.25}W_{0.5}$ alloys

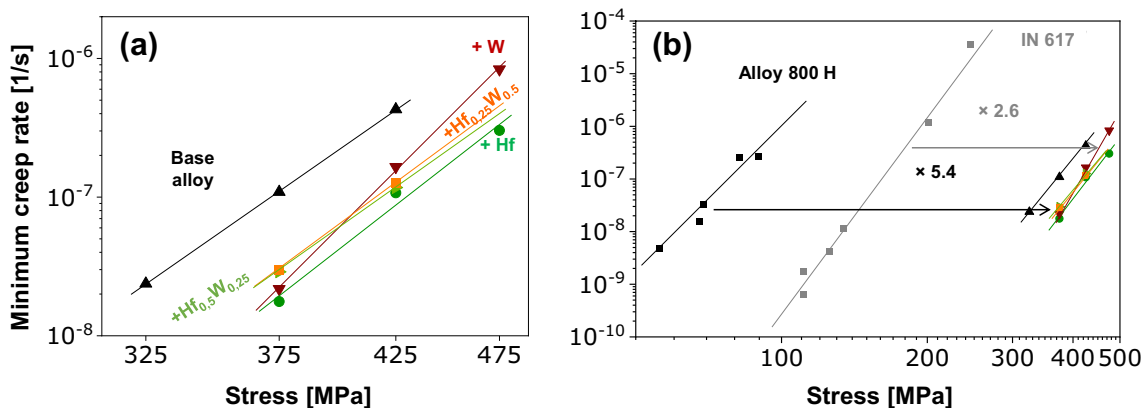


Fig. 7 Norton plots at 750 °C a) of the base alloy and the four modified alloys with Hf and W and b) comparing with commercial alloys Alloy 800 H and IN617, adapted partly from [16]

phase in the W alloy has a higher influence on the creep behaviour than the γ' cube' shape. This is also in agreement with the microstructural observations made from Fig. 1, from which it was concluded that the volume fraction of the Heusler phase plays a great role. The influence of the Heusler phase's shape has already been discussed before [16]. These findings are important to consider for the design of future alloys of this family.

Summary

Compositionally complex alloy $\text{Al}_{10}\text{Co}_{25}\text{Cr}_8\text{Fe}_{15}\text{Ni}_{36}\text{Ti}_6$ was fine-tuned with trace elements Hf and W in order to relate the microstructure of the obtained alloys to the lattice misfit and the creep rate. The following can be summarized:

- The microstructures of all investigated alloys consist of a γ -matrix, γ' -precipitates and a Heusler phase. The shapes of the γ' -precipitates changes from rounded to angular precipitates according to their W and Hf amount. The shapes of the γ' -precipitates in the alloys with more Hf are more angular than those in the alloys with more W.
- The lattice parameters of γ and γ' of the four modified alloys at temperatures from room temperature to almost 930 °C are mostly higher than those of the base alloy $\text{Al}_{10}\text{Co}_{25}\text{Cr}_8\text{Fe}_{15}\text{Ni}_{36}\text{Ti}_6$. It can be concluded that the elements Hf and W, while having a phase partitioning preference, also increase the lattice parameter of the other phase.
- All alloys have a positive lattice misfit in the range of 1.0×10^{-3} to 4.4×10^{-3} .
- The lattice misfit directly affects the shape of the γ' -precipitates. The lower the edge radius, the higher the value of the lattice misfit and vice versa.
- The creep rate was confirmed to depend rather sensibly on the volume fraction of the Heusler phase in a given alloy. The shape of the γ' -precipitates, though reproducing the trend from a maximum change in the Hf alloy to minimum in the W alloy, plays a minor role.
- The endured stress for a given creep rate increases in all modified alloys compared to the base alloy by about 13%. The modified alloys with Hf (and thus with a Heusler phase) exhibit a similar creep response and the same Norton exponent. Heusler-free W alloy behaves differently.

Supplementary Information The online version contains supplementary material available at <https://doi.org/10.1007/s44210-022-00009-1>.

Acknowledgements Authors thank the German Research Foundation (DFG) for the financial support through MA7004/1-1, MA7004/1-2,

GL181/50-1 and GL181/50-2, and through the Priority Program SPP2006 “Compositionally Complex Alloys—High Entropy Alloys (CCA-HEA)”. Many thanks to C. Förster and C. Leistner from HZB for help with sample casting and preparation. Authors would also like to acknowledge M. Buchheim and R. Saliwan Neumann for their help with recording SEM pictures, G. Oder for her support during sample preparation and H. Goldbeck for help with etching. Allocation of synchrotron radiation beamtime at the diffraction instrument at KMC-2 beamline at BESSY II as well as the use of the Laue camera in the Quantum Materials Core Lab, Helmholtz-Zentrum Berlin für Materialien und Energie (HZB) is acknowledged.

Funding Open Access funding enabled and organized by Projekt DEAL. The research leading to these results received funding from German Research Foundation under award number 316699240.

Data Availability The datasets generated during and/or analyzed during the current study are available from the corresponding author on reasonable request.

Declarations

Conflict of interests The authors declare that they have no known competing financial interests or personal relationships that could have appeared to influence the work reported in this paper.

Open Access This article is licensed under a Creative Commons Attribution 4.0 International License, which permits use, sharing, adaptation, distribution and reproduction in any medium or format, as long as you give appropriate credit to the original author(s) and the source, provide a link to the Creative Commons licence, and indicate if changes were made. The images or other third party material in this article are included in the article's Creative Commons licence, unless indicated otherwise in a credit line to the material. If material is not included in the article's Creative Commons licence and your intended use is not permitted by statutory regulation or exceeds the permitted use, you will need to obtain permission directly from the copyright holder. To view a copy of this licence, visit <http://creativecommons.org/licenses/by/4.0/>.

References

1. T.E. Norgate, S. Jahanshahi, W.J. Rankin, Assessing the environmental impact of metal production processes. *J. Cleaner Prod.* **15**(8–9), 838–848 (2007). <https://doi.org/10.1016/j.jclepro.2006.06.018>
2. Shi, Yunzhu, Yang, Bin, Liaw, K. Peter, Corrosion-resistant high-entropy alloys: a review. *Metals* **7**(2), 43 (2017). <https://doi.org/10.3390/met7020043>
3. M.H. Tsai, J.W. Yeh, High-entropy alloys: a critical review. *Mater. Res. Lett.* **2**(3), 107–123 (2014). <https://doi.org/10.1080/21663831.2014.912690>
4. Sandmeyer Steel Company. Nickel Alloy Plate - Alloy 800H/800HT. <https://www.sandmeyersteel.com/A800-A800H-A800AT.html>. Accessed 24 March 2022
5. Special Metals. <http://www.specialmetals.com/documents/Inconel%20alloy%20617.pdf> Accessed 20 March 2022
6. The Version TCCR, ThermoCalc Software AB. Stockholm, Sweden. <http://www.thermocalc.com>
7. Thermotech Ni-based Superalloys Database, TTNI7 (Version 7.0). Stockholm, Sweden.
8. A.M. Manzoni, S. Singh, H.M. Daoud, R. Popp, R. Völkl, U. Glatzel, N. Wanderka, On the path to optimizing the

- Al-Co-Cr-Cu-Fe-Ni-Ti high entropy alloy family for high temperature applications. *Entropy* **18**(4), 104 (2016). <https://doi.org/10.3390/e18040104>
9. A.M. Manzoni, S. Haas, J.M. Yu, H.M. Daoud, U. Glatzel, H. Aboufadi, F. Mücklich, R. Duran, G. Schmitz, D.M. Töbrens, S. Matsumura, F. Vogel, N. Wanderka, Evolution of gamma/gamma' phases, their misfit and volume fractions in Al₁₀Co₂₅Cr₈Fe₁₅Ni₃₆Ti₆ compositionally complex alloy. *Mater. Charact.* **154**, 363–376 (2019). <https://doi.org/10.1016/j.matchar.2019.06.009>
 10. F. Otto, A. Dlouhy, Ch. Somsen, H. Bei, G. Eggeler, E.P. George, The influences of temperature and microstructure on the tensile properties of a CoCrFeMnNi high-entropy alloy. *Acta Mater.* **61**(15), 5743–5755 (2013). <https://doi.org/10.1016/j.actamat.2013.06.018>
 11. A.V. Kuznetsov, D.G. Shaysultanov, N.D. Stepanov, G.A. Salishchev, O.N. Senkov, Tensile properties of an AlCrCuNiFeCo high-entropy alloy in as-cast and wrought conditions. *Mater. Sci. Eng.* **533**, 107–118 (2012). <https://doi.org/10.1016/j.msea.2011.11.045>
 12. H.M. Daoud, A.M. Manzoni, N. Wanderka, U. Glatzel, High-temperature tensile strength of Al₁₀Co₂₅Cr₈Fe₁₅Ni₃₆Ti₆ compositionally complex alloy (high-entropy alloy). *JOM* **67**, 2271–2277 (2015). <https://doi.org/10.1007/s11837-015-1484-7>
 13. S. Haas, A.M. Manzoni, F. Krieg, U. Glatzel, Microstructure and mechanical properties of precipitate strengthened high entropy alloy Al₁₀Co₂₅Cr₈Fe₁₅Ni₃₆Ti₆ with additions of hafnium and molybdenum. *Entropy* **21**(2), 169 (2019). <https://doi.org/10.3390/e21020169>
 14. A. Manzoni, S. Haas, H. Daoud, U. Glatzel, C. Förster, N. Wanderka, Tensile behavior and evolution of the phases in the Al₁₀Co₂₅Cr₈Fe₁₅Ni₃₆Ti₆ compositionally complex/high entropy alloy. *Entropy* **20**(9), 646 (2018). <https://doi.org/10.3390/e20090646>
 15. A.M. Manzoni, H.M. Daoud, R. Voelkl, U. Glatzel, N. Wanderka, Influence of W, Mo and Ti trace elements on the phase separation in Al₈Co₁₇Cr₁₇Cu₈Fe₁₇Ni₃₃ based high entropy alloy. *Ultramicroscopy* **159**(2), 265–271 (2015). <https://doi.org/10.1016/j.ultramic.2015.06.009>
 16. S. Haas, A.M. Manzoni, M. Holzinger, U. Glatzel, Influence of high melting elements on microstructure, tensile strength and creep resistance of the compositionally complex alloy Al₁₀Co₂₅Cr₈Fe₁₅Ni₃₆Ti₆. *Mater. Chem. Phys.* **274**, 125163 (2021). <https://doi.org/10.1016/j.matchemphys.2021.125163>
 17. A.M. Manzoni, S. Haas, H. Kropf, J. Duarte, C.T. Cakir, F. Dubois, D. Töbrens, U. Glatzel, Temperature evolution of lattice misfit in Hf and Mo variations of the Al₁₀Co₂₅Cr₈Fe₁₅Ni₃₆Ti₆ compositionally complex alloy. *Scripta Mater.* **188**, 74–79 (2020). <https://doi.org/10.1016/j.scriptamat.2020.07.013>
 18. A.M. Manzoni, F. Dubois, M.S. Mousa, C. von Schlippenbach, D.M. Töbrens, Y. Yesilcicek, E. Zaiser, R. Hesse, S. Haas, U. Glatzel, On the formation of eutectics in variations of the Al₁₀Co₂₅Cr₈Fe₁₅Ni₃₆Ti₆ compositionally complex alloy. *Metall. and Mater. Trans. A* **52**(1), 143–150 (2021). <https://doi.org/10.1007/s11661-020-06091-7>
 19. Helmholtz-Zentrum Berlin für Materialien und Energie. KMC-2: an X-ray beamline with dedicated diffraction and XAS endstations at BESSY II. *Journal of Large-Scale Research Facilities* (2016). <https://doi.org/10.17815/jlsrf-2-65>
 20. R.C. Reed, *The Superalloys* (Fundamentals and Applications. Cambridge University Press, Cambridge, 2006)
 21. Origin(Pro) (Version 2017). Northampton, MA, USA: OriginLab Corporation.
 22. J. Schindelin, I. Arganda-Carreras, E. Frise, V. Kaynig, M. Longair, T. Pietzsch, S. Preibisch, C. Rueden, S. Saalfeld, B. Schmid, J.-Y. Tinevez, D.J. White, V. Hartenstein, K. Eliceiri, P. Tomancak, A. Cardona, Fiji: an open-source platform for biological-image analysis. *Nat. Methods* **9**, 676 (2012). <https://doi.org/10.1038/nmeth.2019>
 23. I. Arganda-Carreras, V. Kaynig, C. Rueden, K.W. Eliceiri, J. Schindelin, A. Cardona, H.S. Seung, Trainable Weka Segmentation: a machine learning tool for microscopy pixel classification. *Bioinformatics* **33**(15), 2424–2426 (2017). <https://doi.org/10.1093/bioinformatics/btx180>
 24. S. Haas, Einfluss hochschmelzender Legierungselemente auf Mikrostruktur und Hochtemperaturbeständigkeit einer Legierung mit komplexer Zusammensetzung Al₁₀Co₂₅Cr₈Fe₁₅Ni₃₆Ti₆. PhD thesis, University Bayreuth, 2020
 25. J. Svoboda, P. Lukáš, Model of creep in <001>-oriented superalloy single crystals. *Acta Mater.* **46**(10), 3421–3431 (1998). [https://doi.org/10.1016/S1359-6454\(98\)00043-3](https://doi.org/10.1016/S1359-6454(98)00043-3)
 26. B. Geddes, H. Leon, X. Huang, *Superalloys: alloying and performance*. ASM International (2010)
 27. T. Maebashi, M. Doi, Coarsening behaviours of coherent γ' and γ precipitates in elastically constrained Ni–Al–Ti alloys. *Mater. Sci. Eng., A* **373**(1–2), 72–79 (2004). <https://doi.org/10.1016/j.msea.2003.12.064>
 28. H. Mughrabi, The importance of sign and magnitude of γ/γ' lattice misfit in superalloys—with special reference to the new γ'-hardened cobalt-base superalloys. *Acta Mater.* **81**, 21–29 (2014). <https://doi.org/10.1016/j.actamat.2014.08.005>

Publisher's Note Springer Nature remains neutral with regard to jurisdictional claims in published maps and institutional affiliations.